The Geographical Locations of Southern Hemisphere Storm Tracks: Linear Theory

J. S. FREDERIKSEN

CSIRO, Division of Atmospheric Research, Aspendale, Victoria, Australia

(Manuscript received 19 June 1984; in final form 11 December 1984)

ABSTRACT

The instability properties of a three-dimensional climatological January Southern Hemisphere flow field are examined using a five-level spherical quasi-geostrophic spectral model. The growth rates, phase frequencies, disturbance streamfunctions and eddy momentum and heat fluxes are studied for the eight fastest growing modes, all of which are monopole cyclogenesis modes. There is reasonable agreement between instability theory and observations as far as the geographical locations of the storm tracks and eddy fluxes are concerned. The principal storm track is located in the eastern part of the hemisphere slightly downstream and poleward of the jet stream maxima. The usual vertical structure problem of instability theory occurs with the theoretical disturbance streamfunctions and eddy fluxes being relatively too large at the surface compared with values at the tropopause.

1. Introduction

In recent years, observational studies of Northern Hemisphere variability have focused on the local preferred geographical regions of the development of transient cyclone-scale disturbances and their associated eddy fluxes as well as on low frequency fluctuations (Blackmon, 1976; Blackmon *et al.*, 1977; Lau *et al.*, 1978; Lau and Oort, 1981; Lau 1978, 1979; White, 1982). Theoretical studies of the role that the planetary-scale waves in the atmospheric flow patterns play in determining the geographical locations of the Northern Hemisphere storm tracks have also been carried out (Frederiksen, 1979a, 1983). The results obtained from this three-dimensional instability theory with zonally varying basic states were found to be in quite good agreement with observations. Both the observed and theoretical regions of preferential development occur slightly downstream and poleward of the jet stream maxima and it was found that this phenomenon could be explained in terms of general instability criteria (Frederiksen, 1980, and references therein).

For the Southern Hemisphere there has been a similar interest in elucidating the geographical locations of the storm tracks and the horizontal structures of eddy fluxes from observations (Trenberth, 1979, 1980, 1981, 1982, 1984; van Loon, 1980; Physick, 1981). A brief review of the earlier observational studies is given by Trenberth (1981). As yet there have been no theoretical studies of Southern Hemisphere climatological flows using instability models with three-dimensional basic states. However, Trenberth (1981, 1984) noted that the location of the observed Southern Hemisphere storm track, slightly downstream and poleward of the jet stream maxima, was also consistent with the results of three-dimensional instability studies with idealized basic states and with expectations based on general instability criteria (Frederiksen, 1979a, 1980).

Trenberth (1981) examined the annual average eddy activity and subsequently (Trenberth, 1982) considered it for the separate summer and winter seasons. He found that there was little change in the level of eddy activity from summer to winter and almost no change in the latitude of the maximum variance of the geopotential heights and meridional velocities as shown in Figs. 3 and 6 (Trenberth, 1982). Thus the Southern Hemisphere storm tracks show considerably less variation with season than those in the Northern Hemisphere.

The purpose of this article is to examine directly the instability properties of three-dimensional Southern Hemisphere climatological flow. In view of the fact that the main storm track does not vary greatly with season we shall confine our study to a January climatological basic state. The characteristics of the model used for the study and the truncation scheme are briefly discussed in Section 2; details of the basic state are described in Section 3. The growth rates, phase frequencies, disturbance streamfunctions and eddy momentum and heat fluxes of the eight fastest growing modes are analyzed and compared with observations in Section 4. The conclusions are summarized in Section 5.

2. Model details

We use the same spherical five-level quasi-geostrophic model for this study as in Frederiksen (1983);

the model incorporates drag $-K^d(p)\nabla^2\psi$ and diffusion $-K^r\nabla^6\psi$ where ψ is the streamfunction, $K^d(p) = 8.39 \times 10^{-7}$ s^{-1} at 900 mb and is zero otherwise and $K^r = 2.338 \times 10^{16}$ m^4 s^{-1} at all levels. The streamfunction is specified at odd multiples of 100 mb and the temperature T at even multiples.

The basic state flow field, which is taken to be stationary is expanded in terms of spherical harmonics [Eq. (2.10) of Frederiksen, 1983]. A rhomboidal truncation is used in which ρ, the zonal wavenumber, takes the values $|\rho| = 0, 1, \ldots, 15$ and the total wavenumber $\nu = |\rho| + 1, |\rho| + 3, \ldots, |\rho| + 15$ for the antisymmetric basic-state streamfunctions. The disturbances are also represented by spherical harmonics at each level and have a time dependence $\exp(-i\omega t)$ where $\omega = \omega_r + i\omega_i$ is the complex angular frequency [Eq. (2.11) of Frederiksen, 1983]. For the disturbances, a parallelogrammic truncation is used in which m, the zonal wavenumber, takes the values $m = 0, 1, \ldots, 15$ and n, the total wavenumber, takes the values $n = |m| + 1, |m| + 3, \ldots, |m| + 9$ for the antisymmetric streamfunctions. It would be desirable to be able to increase the resolution. However the present resolution is close to the maximum possible on modern computers with the current formulation in which all eigenvalues are obtained.

The equations are linearized about the basic state and solved as eigenvalue-eigenvector equations for ω and the disturbance spectral coefficients.

3. Basic state

The Southern Hemisphere climatological January flow obtained from monthly averages from 1972 to 1976 as determined by the Australian Bureau of Meteorology analysis is used for the three-dimensional basic state. The geopotential heights which define the 300 and 700 mb basic flows are shown in Figs. 1a, b. These diagrams are very similar to the climatology of Taljaard *et al.* (1969); the 500 mb geopotential height is very similar to that shown in Fig. 1a of Trenberth (1979) for a slightly more extensive data set for January. Figure 1b, in particular, shows the confluent nature of the flow in the Indian Ocean with the trough at high latitudes and a ridge at low latitudes (see also Fig. 1 of Trenberth, 1980). Figures 2a and b show the zonal geostrophic wind components u at 300 and 700 mb corresponding to the geopotential heights in Fig. 1. Again the comparison with earlier climatological studies is close; the strongest westerlies occur in the southern Indian Ocean as in the studies of van Loon (1972, Fig. 5.2), Webster and Curtin (1975, Fig. 2c) and Trenberth (1979, Fig. 3a). The zonally averaged zonal wind[1] is shown in Fig. 3, where $\sigma = p/1000$ is the normalized pressure. There is close qualitative agreement between Fig. 3 and the corresponding results in Fig. 5.6 of van Loon (1972), Fig. 19 of Knittel (1976) and Fig. 1 of Trenberth (1984). The three-monthly summer averages in Newell *et al.* (1972) are also quite similar but the winds there are somewhat less intense as might be expected. In both Figs. 2 and 3 we see that the strongest winds occur at about 45°S. Figure 4 gives the horizontally averaged temperature from which the static stability parameter is calculated using simple vertical finite differences.

[1] The zonally averaged zonal winds in Fig. 1 of Frederiksen (1981a) are slightly displaced in the vertical due to a plotting routine error.

4. Instability of the three-dimensional January flow

The instability properties of the zonally averaged flow for Southern Hemisphere January were considered in a nine-level model by Frederiksen (1981a) and subsequent nonlinear evolution of the disturbances to the mean flow was studied in Frederiksen (1981b, c). For the corresponding three-dimensional flow it is necessary to reduce the vertical resolution in order to solve the eigenvalue-eigenvector problem on existing computers using the present formulation. The fastest growing instability modes obtained with the present five-level model may nevertheless be more realistic when compared with observations and nonlinear integrations than those obtained with higher resolution. This is because instability studies in multilevel models with a large number of levels may produce rather larger growth rates for the small-scale disturbances, which would therefore appear to be most important. However, the short-wavelength disturbances are usually primarily surface disturbances which in the corresponding nonlinear study cease growing much earlier and make a less important contribution to energy spectra than the somewhat longer wavelength disturbances that dominate the growth rate with lesser vertical resolution.

a. Growth rates and phase frequencies

Table 1 shows the growth rates ω_i and phase frequencies ω_r of the eight fastest growing modes for the three-dimensional January basic state. Some of the eight fastest growing modes have very similar properties and have therefore been classified into three classes denoted α, β and γ. We shall only discuss the fastest growing mode from each class in detail. The growth rates in Table 1 are quite similar to those obtained in Frederiksen (1984) for the three-dimensional instantaneous Southern Hemisphere synoptic flows for August and May, but are somewhat less than those found with the nine-level model and zonally averaged basic January climatology in Frederiksen (1981a). This tendency of reduced vertical resolution to reduce growth rates of baroclinic disturbances has previously been discussed (Frederiksen, 1978 and references therein).

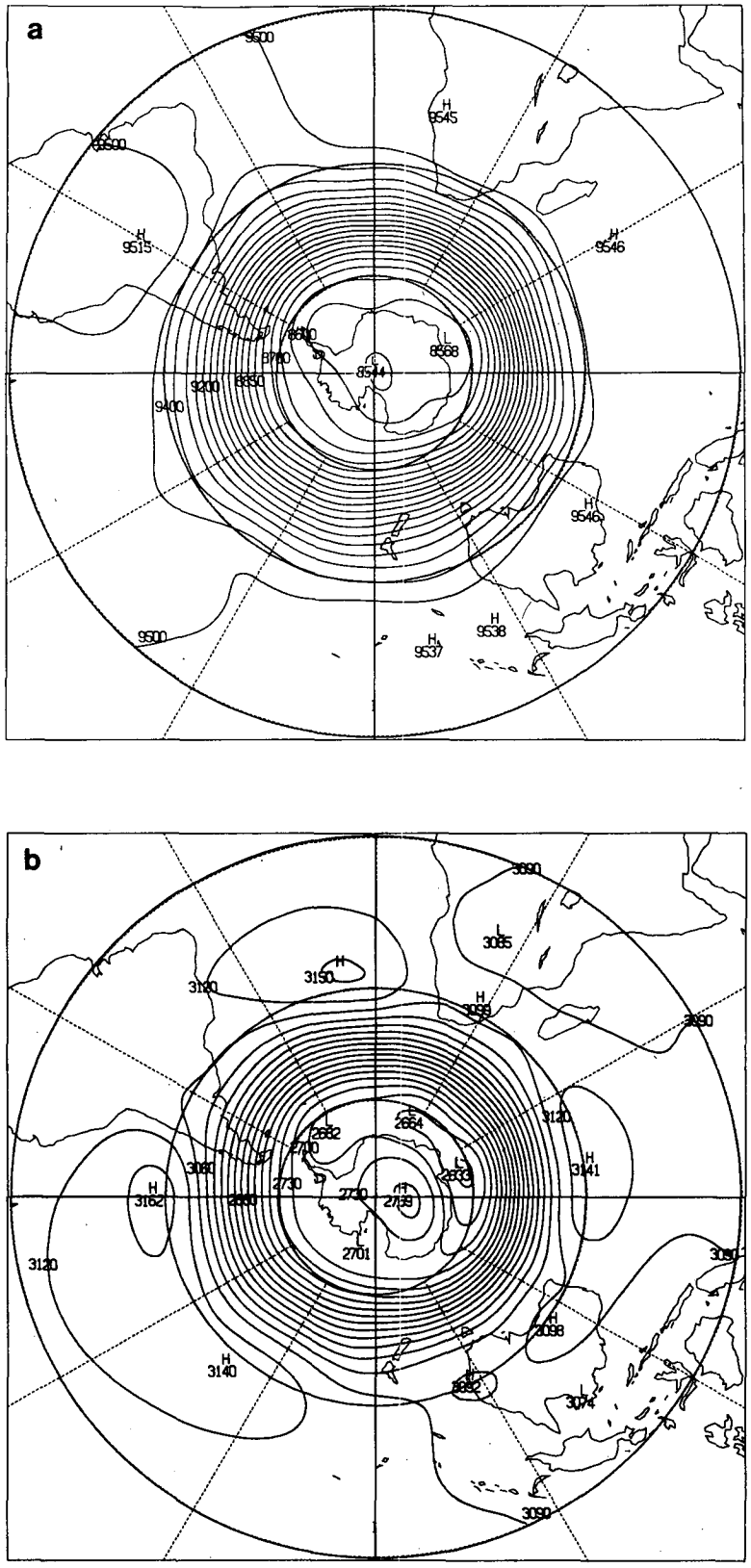

FIG. 1. Geopotential height (m) of (a) 300 mb and (b) 700 mb surface for January climatology.

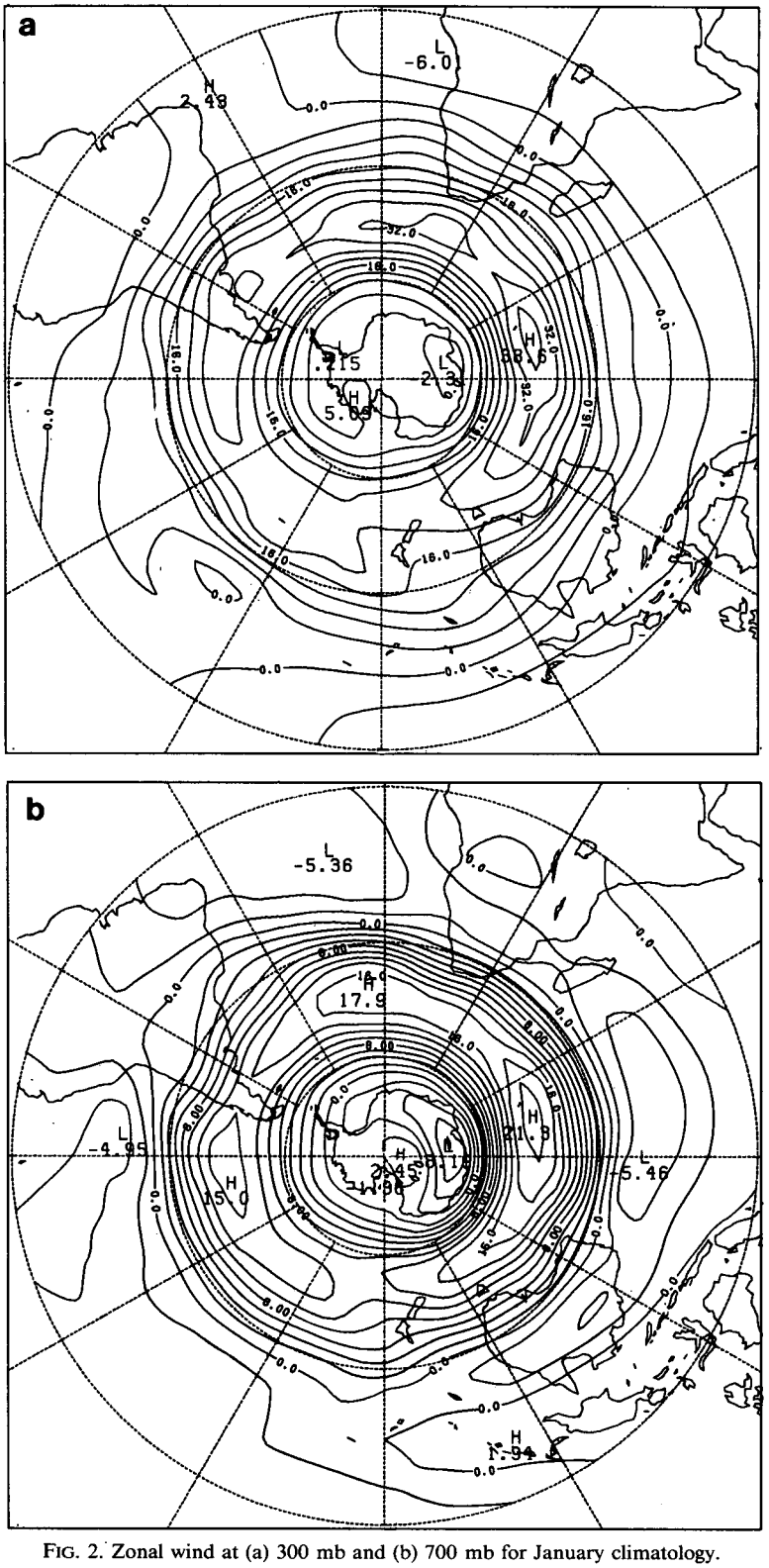

FIG. 2. Zonal wind at (a) 300 mb and (b) 700 mb for January climatology.

b. Disturbance streamfunctions

Figure 5a, b show the 700 mb disturbance streamfunction ψ and the 700 mb random phase ensemble average (RPEA) disturbance streamfunction $\langle\psi^2\rangle^{1/2}$ for the fastest growing mode of class α (mode 1) while Fig. 6a, b show the corresponding quantities for the fastest growing mode of class β (mode 4). For

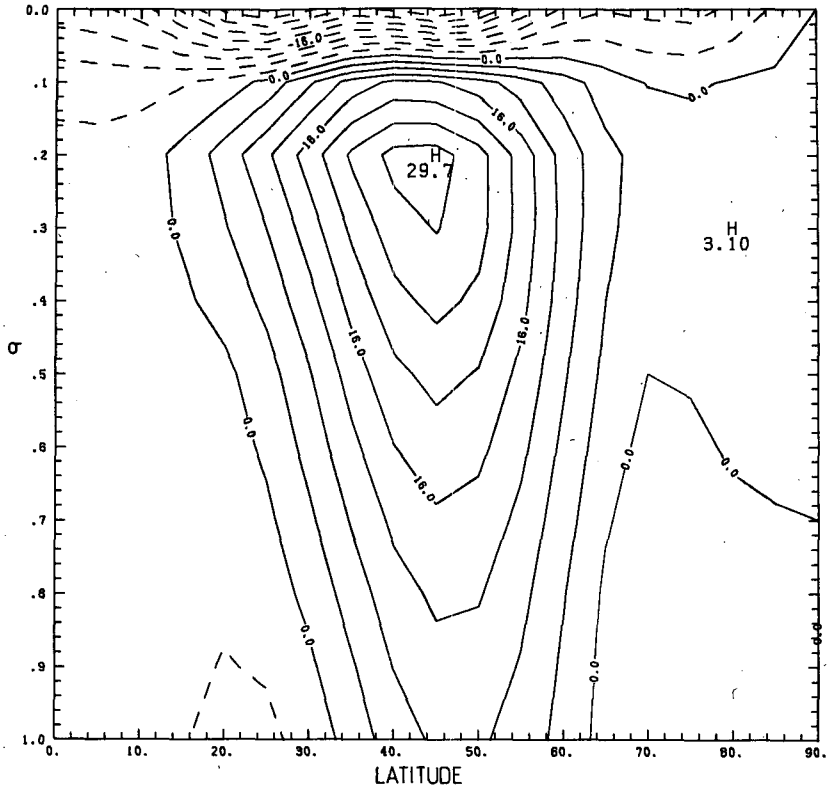

FIG. 3. Zonally averaged zonal wind as a function of normalized pressure σ and latitude for January climatology.

the fastest growing mode of class γ (mode 7) the 700 mb RPEA streamfunction is shown in Fig. 7. The instantaneous disturbance streamfunction ψ has a monopole structure like those in Figs. 5a and 6a with similar effective wavenumber to that of mode 4 in the regions of largest amplitude; they are the same as those shown for the RPEA in Fig. 7. Here the RPEA is obtained by averaging over all possible phases of the disturbance streamfunction; it is defined in Eq. (5.1) of Frederiksen (1983) and is just $2^{-1/2}$ times the

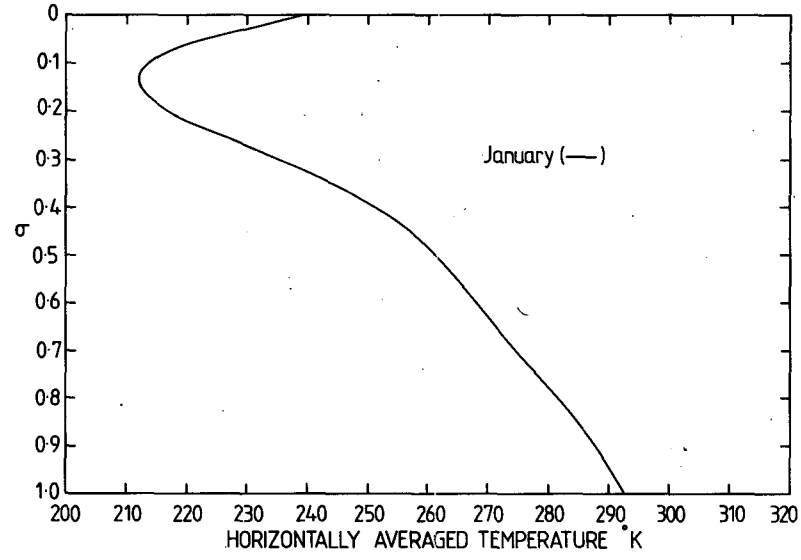

FIG. 4. Profile of the horizontally averaged temperature as a function of normalized pressure σ for January climatology.

TABLE 1. Phase frequencies and growth rates in nondimensional and dimensional units of the eight fastest growing modes. Also shown are the classes to which the different modes belong.

Mode	Class	ω_r	ω_r^d (deg day^{-1})	ω_i	ω_i^d (day^{-1})
1	α	0.307	110.5	0.0529	0.332
2	α	0.356	128.2	0.0525	0.330
3	α	0.261	94.0	0.0489	0.307
4	β	0.394	141.8	0.0470	0.295
5	β	0.424	152.6	0.0419	0.263
6	β	0.464	167.0	0.0393	0.247
7	γ	0.553	199.1	0.0374	0.235
8	β	0.638	229.7	0.0352	0.221

amplitude of the disturbance streamfunction. The vertical structures of the disturbances, as given by the maximum values of the RPEA disturbance streamfunction at each level, are shown in Table 2.

For each of the three modes shown in Figs. 5, 6 and 7 the geographical locations of the RPEA disturbance streamfunctions, with maxima between 45 and 50°S in the Indian Ocean and to the south of Africa and Australia, are consistent with modes of these types making contributions to the observed storm tracks in the Southern Hemisphere summer. Compare, for example, Fig. 11c of Trenberth (1982), which shows the geopotential height variance in the 2–8 day band for summer and Fig. 6b of Trenberth (1982), which shows the variance of the meridional velocity for summer. We also recall that although the winter flows considered in Frederiksen (1984) were instantaneous Southern Hemisphere flows, the cyclogenesis instability modes picked out the main observed storm track characteristic of winter climatology. From Table 2, we see that the vertical penetration of the disturbances to the 300 mb level is considerably less than indicated in the observations of the standard deviation of the meridional wind for December to February in Table 3.6 of Newell *et al.* (1972) and in nonlinear integrations with zonally averaged basic states (Fig. 6c of Frederiksen, 1981b; Fig. 2b of Frederiksen, 1981c). Thus the usual vertical structure problem (Frederiksen, 1981a, Section 5a and references therein) of linear instability solutions, viz. that the amplitudes of the disturbances are too small near the tropopause compared with those at the surface, also occurs with three-dimensional basic climatological states. The largest ratio of the 300 to 900 mb RPEA disturbance maxima occurs for the fastest growing mode of class β. We might therefore expect that, in corresponding nonlinear integrations started from the same three-dimensional basic state perturbed by these disturbances, the α and γ modes would undergo larger changes than the β mode and that these would occur at earlier stages of their life cycles. In this sense, the β-mode may be regarded as the most representative and realistic of the eight fastest growing modes, and in the subsequent subsections we shall concentrate on it.

The β-mode has a slight westward tilt with height between 900 and 300 mb and this is reflected in the RPEA streamfunction for which the maximum value has a 10° westward tilt between 900 and 300 mb. At 100 mb the maximum amplitude of the disturbance occurs further upstream at 90°E long. The γ-mode has a similar coherence in the vertical to that of the β-mode, but this now extends to 100 mb with the disturbance streamfunction and the maximum of the RPEA streamfunction having about 10° westward tilt between 900 and 100 mb. The shallow α-mode has somewhat less coherence in the vertical than either the β- or γ-modes; it appears to be more sensitive to local horizontal shears at different levels. The largest amplitudes occur in the eastern part of the hemisphere at all levels, as is the case at 700 mb shown in Fig. 5. However at 300 and 500 mb secondary and tertiary maxima occur over South America near 40°S. In addition, at 900 mb the maximum of the RPEA streamfunction occurs south of Australia in a position very similar to the secondary maximum at 700 mb.

In previous studies of idealized (Frederiksen, 1978) and Northern Hemisphere three-dimensional flows (Frederiksen, 1979a, 1983), it has been possible to relate the regions of maximum amplitude of the disturbance streamfunctions, in cases where barotropic instability is relatively unimportant, to a generalization of Phillips' (1954) criterion for instability (Frederiksen, 1980). That is, the most intense development tends to occur slightly downstream of the position where the difference between the vertical wind shear and the general instability criterion is a maximum. Because the instability criterion increases towards the equator, this maximum "excess shear" tends to occur slightly poleward of the regions of maximum zonal winds.

Trenberth (1981, 1982) found that the relation between the observed Southern Hemisphere jet streams and the location of the main storm track also fits in quite well with the results expected on the basis of the general instability criterion and the qualitative results of three-dimensional instability calculations. We note, however, that compared with the Northern Hemisphere flows and with the idealized flows studied (Frederiksen, 1979a, 1980, 1983) the main jet stream in the Southern Hemisphere is less localized. This results in the main storm track in the Indian Ocean being more extensive with minimum amplitudes occurring over a larger region. Further the poleward shift of the main storm track relative to the jet axis appears to be less than for the Northern Hemisphere observations. (Blackmon *et al.*, 1977, Lau, 1978).

For each of the modes of classes α, β and γ, the maximum RPEA streamfunctions at 900 mb occur downstream of the jetstream maximum in the Indian Ocean, but the extent of downstream displacement depends on the particular mode. For mode β and γ this downstream displacement occurs at all levels.

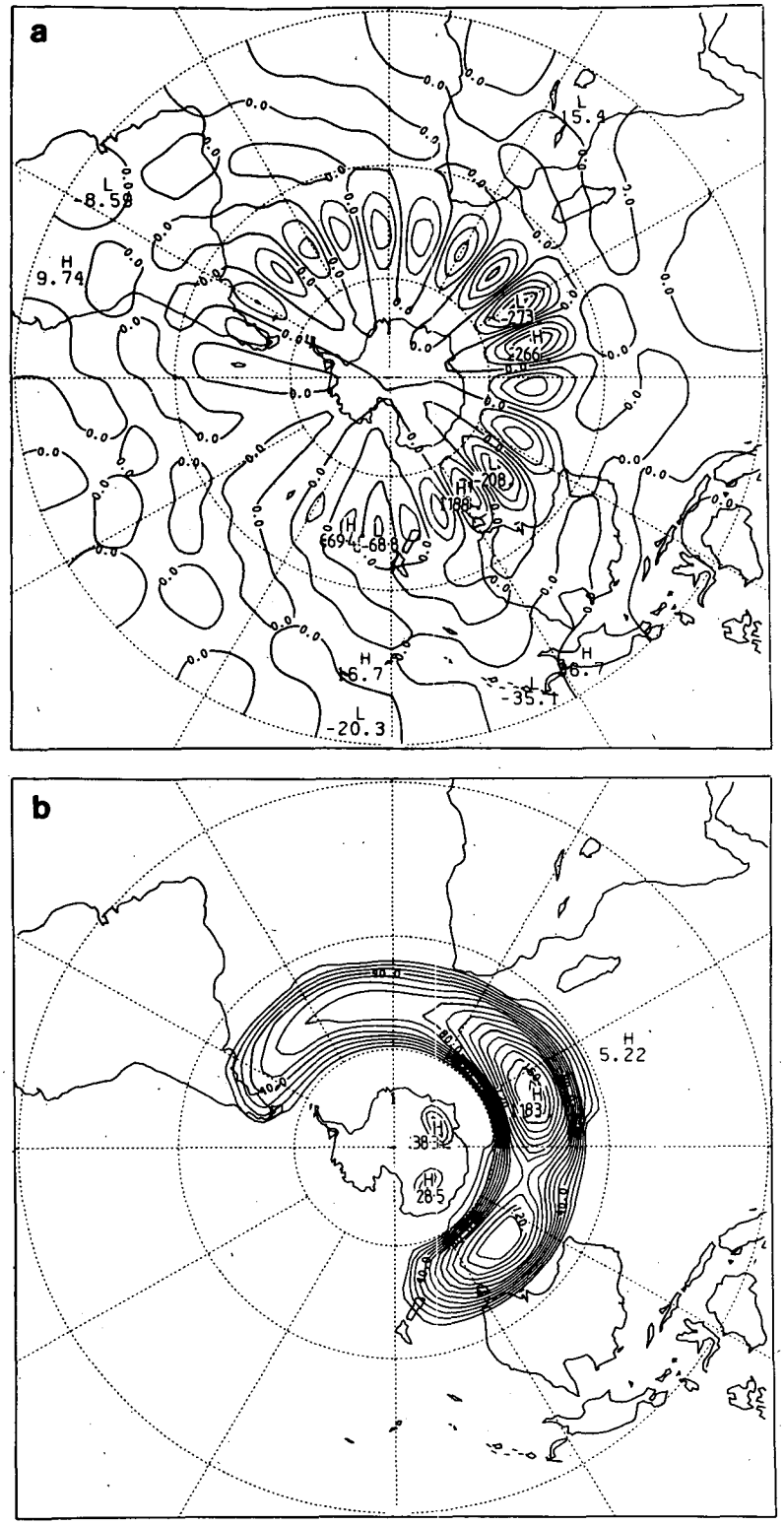

FIG. 5. (a) Disturbance streamfunction and (b) RPEA disturbance streamfunction at 700 mb for mode 1 (of class α).

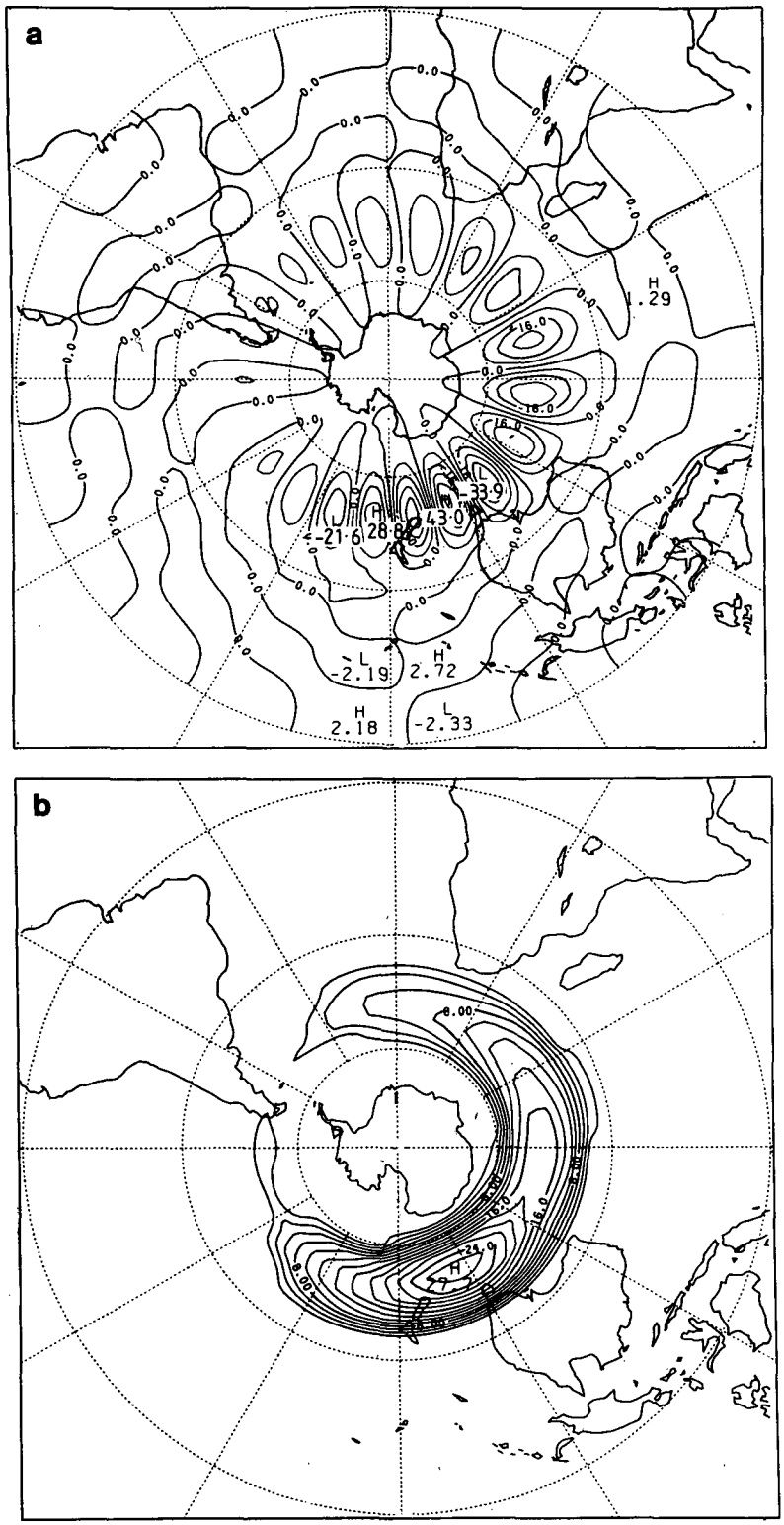

FIG. 6. As in Fig. 5 but for mode 4 (of class β).

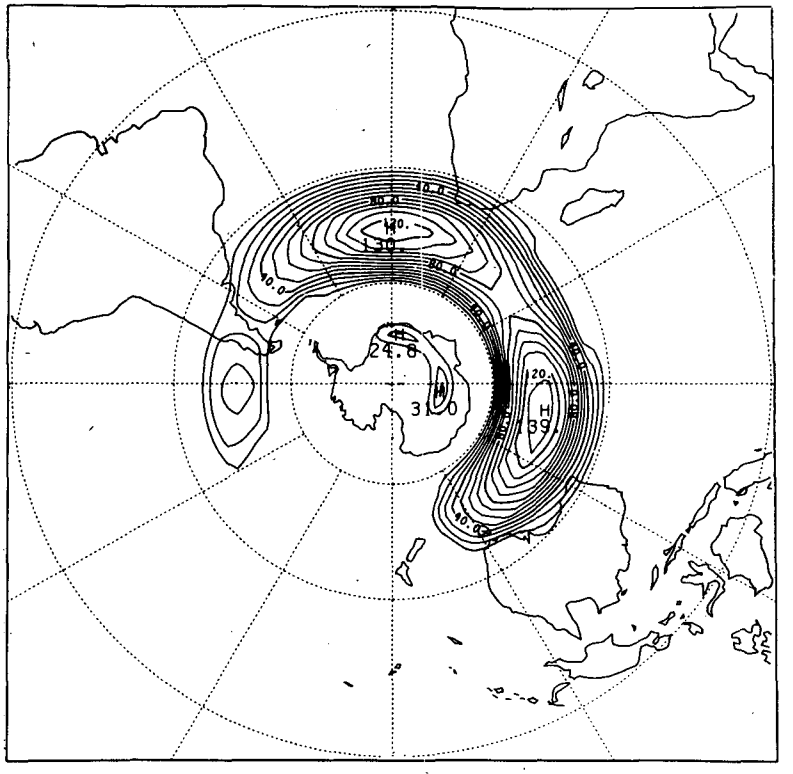

FIG. 7. As in Fig. 5b but for mode 7 (of class γ).

For the α-mode, we see from Fig. 5 that at 700 mb the primary maximum in fact occurs very close to the jet maximum with a secondary maximum located downstream south of Australia. At other levels, the primary maximum occurs either near the jet stream maximum or downstream south of Australia. For the instability results the poleward displacement of the storm tracks is rather slight as was the case for the zonally averaged results for which the disturbance streamfunction amplitude is shown in Fig. 6a of Frederiksen (1981a).

c. Eddy momentum fluxes

Figure 8a, b show the RPEA eddy momentum fluxes $\langle uv \cos^2\phi \rangle$ where ϕ is latitude at 300 and 700 mb respectively for mode β while Fig. 9a, b show the corresponding quantities for mode γ. The largest poleward (positive) and equatorward (negative) momentum fluxes at each level are shown in Table 3 for the fastest growing modes of each of the classes α, β and γ. For mode β, the weaker equatorward flux at 300 mb is centered slightly south of the stronger poleward fluxes, producing a convergence of momentum flux into the jet stream maximum. At the lower levels however the equatorward and poleward fluxes are centered on practically the same latitudes as shown for 700 mb in Fig. 8b. For the γ-mode, the maximum eddy fluxes again occur in the storm tracks and both poleward and equatorward components are centered at very similar latitudes. The same applies for the fastest growing α-mode (not shown) for which the largest eddy fluxes occur in the southern Indian Ocean and south of Australia. As might be expected from the discussion of the disturbance streamfunction for this mode, the eddy momentum fluxes also show less vertical coherence than for the β and γ modes.

The observed characteristics of eddy momentum fluxes by transient eddies in the Southern Hemisphere are given in Fig. 19a of Trenberth (1981) for the whole year and in Fig. 9b of Trenberth (1982) for the summer season. Poleward fluxes are found to occur north of 50°S with equatorward fluxes at higher latitudes with maximum convergence in the southern Indian Ocean. Comparing the theoretical results with

TABLE 2. The maximum values of the RPEA disturbance streamfunctions for modes 1, 4 and 7. The normalization is 1000 arbitrary units.

	Mode		
σ	1	4	7
0.1	69	152	68
0.3	285	755	480
0.5	427	861	665
0.7	1000	837	818
0.9	1000	1000	1000

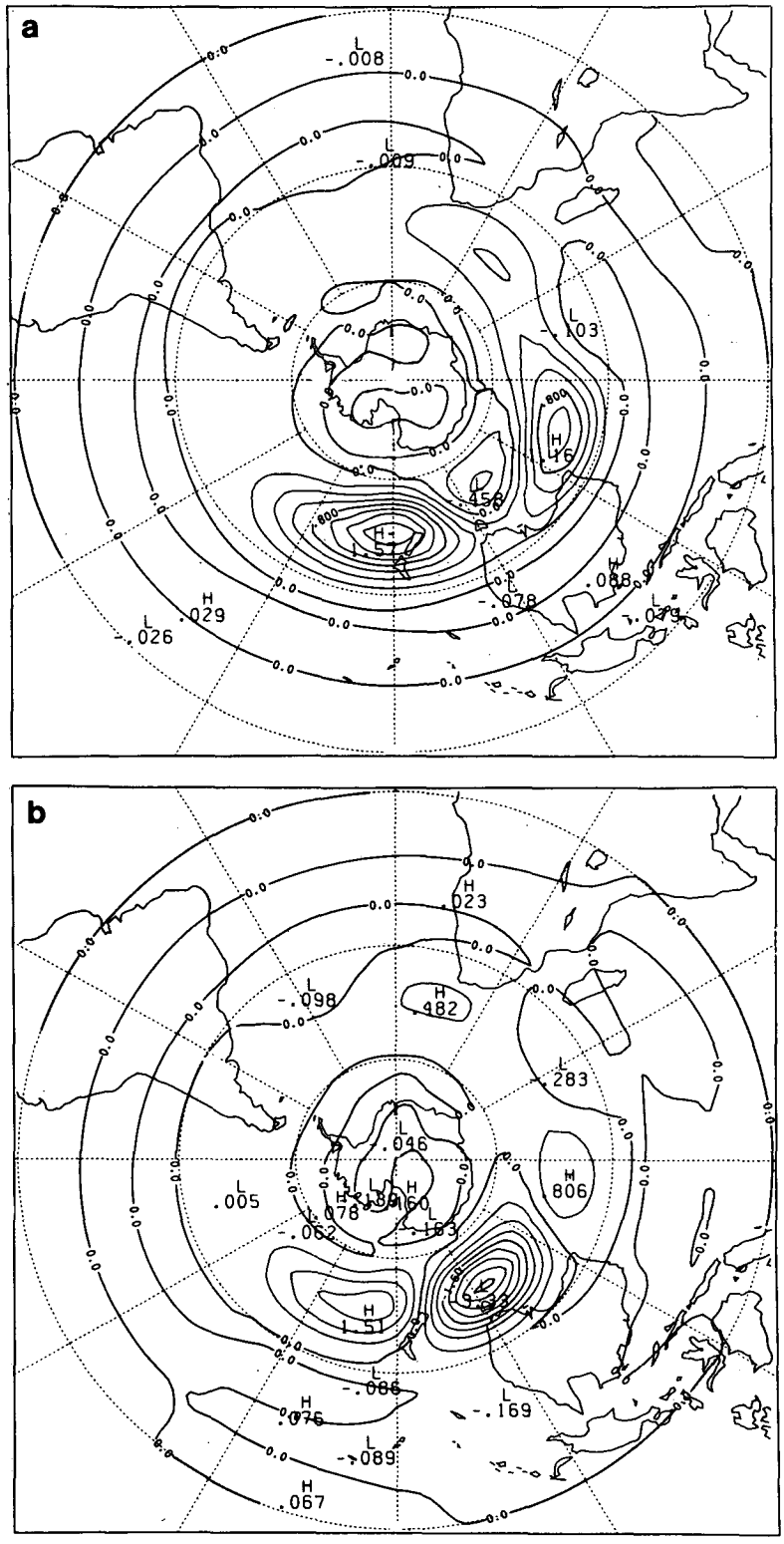

FIG. 8. RPEA momentum flux $\langle uv \cos^2\phi \rangle$ at (a) 300 mb and (b) 700 mb for mode 4 (of class β).

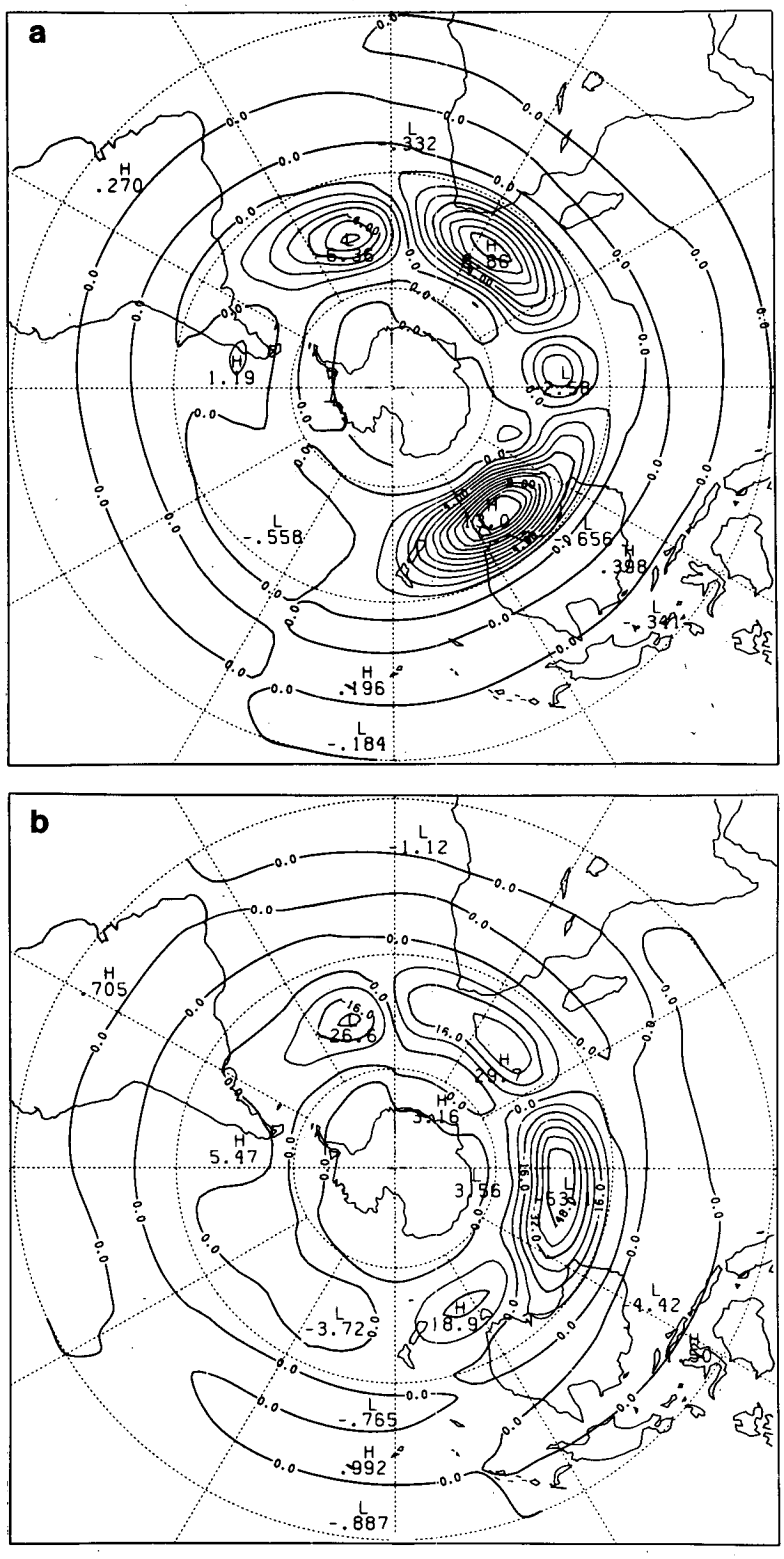

FIG. 9. As in Fig. 8 but for mode 7 (of class γ).

TABLE 3. The largest poleward (positive) and equatorward (negative) RPEA eddy momentum fluxes $\langle uv \cos^2\phi \rangle$ for modes 1, 4 and 7.

	Mode					
σ	1		4		7	
0.1	−1	7	−3	36	−1	4
0.3	−75	118	−128	439	−95	194
0.5	−263	218	−796	542	−451	394
0.7	−1000	520	−930	422	−793	443
0.9	−526	666	−869	1000	−754	1000

the observations, it is clear that while instability theory produces momentum fluxes in approximately the right geographical locations, the juxtaposition of the poleward and equatorward fluxes is in general not quite right. A similar problem occurred in the Atlantic Ocean in a study of the instability properties of a three-dimensional Northern Hemisphere January flow (Frederiksen, 1983). There the momentum fluxes of the fastest and second fastest growing modes had the equatorward component in the Atlantic centered at practically the same latitude as the poleward component, rather than being to the north of it. In a subsequent nonlinear study starting from the same Northern Hemisphere January flow perturbed by the fastest growing instability mode (Frederiksen and Puri, 1985) it is found that the equatorward component of the momentum flux quickly takes up its position to the north of the poleward component. Thus, nonlinear effects can improve the positioning of the eddy flux components. It may also be that increased horizontal resolution would improve the results since in previous studies with idealized flows (Frederiksen, 1979a,b, 1980) the equatorward fluxes were located poleward of the poleward eddy momentum fluxes.

Comparing the results in Table 3 with the observations of zonally averaged eddy momentum fluxes in Fig. 4.9 of Newell *et al.* (1972) for December to February we see that the vertical structure problem occurs for each of the three modes. That is, the eddy momentum fluxes at 300 mb are too weak compared with those at the lowest level as was the case for the modes growing on the zonally averaged January basic state in Frederiksen (1981a).

d. Eddy heat fluxes

The RPEA eddy heat flux $\langle vT \cos\phi \rangle$ at 800 mb for mode β is shown in Fig. 10; Table 4 gives the largest poleward (positive) and equatorward (negative) eddy heat fluxes for each level and for each of modes α, β and γ. Comparing Figs. 6b and 10 we see that the RPEA eddy heat flux for mode β has a very similar qualitative appearance to the RPEA disturbance streamfunction with maximum value downstream and slightly poleward of the jet stream maxi-

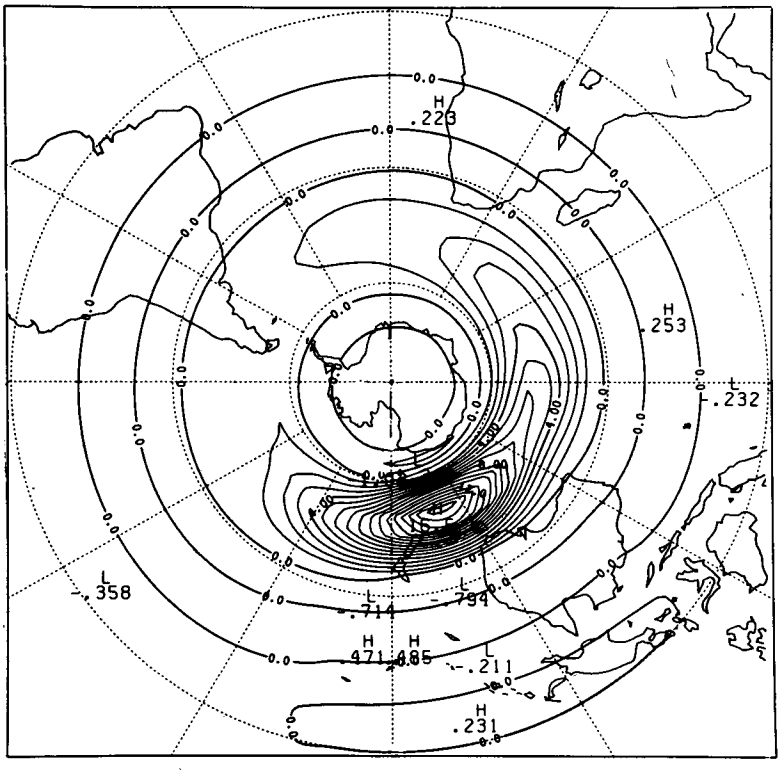

FIG. 10. RPEA heat flux $\langle vT \cos\phi \rangle$ at 800 mb for mode 4 (of class β).

TABLE 4. As in Table 3 but for eddy heat fluxes $\langle vT\cos\phi\rangle$.

	Mode					
σ	1		4		7	
0.2	−3	2	−1	18	−1	5
0.4	−8	46	−14	98	−12	63
0.6	−321	75	−30	278	−31	183
0.8	−108	1000	−101	1000	−92	1000

mum. The position of the largest poleward heat flux tilts westward with height by nearly 30° between 800 and 400 mb. At 200 mb the maximum occurs at about 100°E longitude, reflecting the behavior of the maximum RPEA streamfunction in the upper levels.

For the fastest growing mode of class γ, the RPEA eddy heat flux has at each level a primary poleward maximum in the Indian Ocean and a secondary maximum south of Africa at the latitude of the storm track. As for mode β, the equatorward fluxes are relatively small.

The eddy heat fluxes for the α-mode again have largest magnitudes in the storm tracks. In this case, relatively large equatorward heat fluxes also occur at 600 mb in the Indian Ocean due to the greater sensitivity of the α-mode to local horizontal shears at each level.

The geographical locations and vertical structure of eddy heat fluxes in the Southern Hemisphere were analyzed from observations by van Loon (1980). He also discussed the difficulties of obtaining accurate statistics for eddy heat fluxes in the Southern Hemisphere. Figure 4 of van Loon shows the horizontal distribution of eddy heat flux for summer at 850 mb. Again there is quite reasonable agreement between the theoretical results, particularly for the β and γ modes, and the observations. Both theoretical and observed maximum poleward heat fluxes occur in the storm tracks in the eastern part of the hemisphere between 45 and 50°S. In his Fig. 2, van Loon also gives the vertical structure of the zonally averaged transient eddy heat flux for summer and compares it with the results in Table 7.2 of Newell *et al.* (1974). Newell *et al.* show the sum of the eddy heat fluxes by stationary and transient eddies. The contribution from stationary eddies is small (see, e.g., Webster and Curtin, 1974; Simmonds and Lin, 1983), but despite this the results for the two studies differ by an order of magnitude between 200 and 300 mb. Nevertheless, irrespective of which data set is used, it is clear that the theoretical eddy heat fluxes are too weak in the upper troposphere in relation to near the surface compared with the observations.

5. Conclusions

The instability properties of a three-dimensional climatological Southern Hemisphere flow field for January, taken from monthly averages from 1972 to 1976, have been obtained using a five-level quasi-geostrophic model incorporating spherical geometry. We have studied the growth rates, phase frequencies, disturbance streamfunctions and eddy momentum and heat fluxes for the eight fastest growing modes which have been classified into three classes, denoted α, β and γ, in which the modes have similar properties. The modes are all essentially monopole cyclogenesis modes with relatively large growth rates and phase frequencies and which have largest amplitudes in the observed regions of the storm tracks in the eastern part of the hemisphere near 50°S, particularly in the Indian Ocean and south of Australia. The disturbances have the usual westward tilt with height of baroclinic modes and their maxima are in general located slightly downstream and poleward of the jet stream maxima consistent with expectations based on general instability criteria (Frederiksen, 1980). The geographical locations of the eddy momentum and heat fluxes are also in general agreement with the observations (van Loon, 1980; Trenberth, 1982). The juxtaposition of the theoretical poleward and equatorward eddy momentum fluxes is however not very realistic and the reasons for this have been discussed.

The Southern Hemisphere January jet stream is more nearly zonally symmetric than that of the Northern Hemisphere. This results in both the observed and theoretical storm tracks as determined by eddy activity being more extensive with maximum amplitudes of eddy quantities occurring over a larger region. The vertical structure problem of instability modes growing on zonally averaged basic states also occurs with the present three-dimensional climatological January flow. That is, disturbance streamfunctions, momentum and heat fluxes are too large near the surface compared with their values at the tropopause. This problem is most prevalent for the modes of class α and least for those of class β, for which the most realistic results are obtained.

Inclusion of nonlinear effects is expected to increase the vertical penetration of the modes as in corresponding studies with zonally averaged basic flows (Frederiksen, 1981b,c). We also note that in studies of the development of initial localized disturbances rather than normal modes (Farrell, 1982; Pierrehumbert, 1984), it is possible under certain circumstances to obtain larger upper-level amplitudes even within linear theory.

Acknowledgments. It is a pleasure to thank Steve Kepert for assistance and Sue Webdale for typing the manuscript.

REFERENCES

Blackmon, M. L., 1976: A climatological spectral study of the 500 mb geopotential height of the Northern Hemisphere. *J. Atmos. Sci.*, **33**, 1607–1623.

——, J. M. Wallace, N. Lau and S. L. Mullen, 1977: An observational study of the Northern Hemisphere wintertime circulation. *J. Atmos. Sci.*, **34,** 1040–1053.

Farrell, B. F., 1982: The initial growth of disturbances in a baroclinic flow. *J. Atmos. Sci.*, **39,** 1163–1686.

Frederiksen, J. S., 1978: Growth rates and phase speeds of baroclinic waves in multi-level models on a sphere. *J. Atmos. Sci.*, **35,** 1816–1826.

——, 1979a: The effect of long planetary waves on the regions of cyclogenesis: Linear theory. *J. Atmos. Sci.*, **36,** 195–204.

——, 1979b: Baroclinic instability of zonal flows and planetary waves in multi-level models on a sphere. *J. Atmos. Sci.*, **36,** 2320–2335.

——, 1980: Zonal and meridional variations of eddy fluxes induced by long planetary waves. *Quart. J. Roy. Meteor. Soc.*, **106,** 63–84.

——, 1981a: Disturbances and eddy fluxes in Southern Hemisphere flows: Linear theory. *J. Atmos. Sci.*, **38,** 673–689.

——, 1981b: Growth and vacillation cycles of disturbances in Southern Hemisphere flows. *J. Atmos. Sci.*, **38,** 1360–1375.

——, 1981c: Scale selection and energy spectra of disturbances in Southern Hemisphere flows. *J. Atmos. Sci.*, **38,** 2573–2584.

——, 1983: Disturbances and eddy fluxes in Northern Hemisphere flows: Instability of three-dimensional January and July flows. *J. Atmos. Sci.*, **40,** 836–855.

——, 1984: The onset of blocking and cyclogenesis in Southern Hemisphere synoptic flows: Linear theory. *J. Atmos. Sci.*, **41,** 1116–1131.

——, and K. Puri, 1985: Nonlinear instability and error growth in Northern Hemisphere three-dimensional flows: Cyclogenesis, onset-of-blocking and mature anomalies. *J. Atmos. Sci.*, **42** (in press).

Knittel, J., 1976: Ein Beitrag zur Klimatologie der Stratosphare der Südhalbkugel. *Meteor. Abhand.*, Ser. A. Monogr., Bandz, Heftl.

Lau, N., 1978: On the three-dimensional structure of the observed transient eddy statistics of the Northern Hemisphere wintertime circulation. *J. Atmos. Sci.*, **35,** 1900–1923.

——, 1979: The structure and energetics of transient disturbances in the Northern Hemisphere wintertime circulation. *J. Atmos. Sci.*, **36,** 982–995.

——, and A. H. Oort, 1981: A comparative study of observed Northern Hemisphere circulation statistics based on GFDL and NMC analyses. Part I: The time-mean fields. *Mon. Wea. Rev.*, **109,** 1380–1403.

——, H. Tennekes and J. M. Wallace, 1978: Maintenance of the momentum flux by transient eddies in the upper troposphere. *J. Atmos. Sci.*, **35,** 139–147.

Newell, R. E., J. W. Kidson, D. G. Vincent and G. J. Boer, 1972: *The General Circulation of the Tropical Atmosphere and Interactions with Extratropical Latitudes, Vol. 1.* MIT Press, 258 pp.

——, —— and ——, 1974: *The General Circulation of the Tropical Atmosphere and Interactions with Extratropical Latitudes, Vol. 2.* MIT Press, 371 pp.

Pierrehumbert, R. T., 1984: Local and global baroclinic instability of zonally varying flow. *J. Atmos. Sci.*, **41,** 2141–2162.

Phillips, N. A., 1954: Energy transformations and meridional circulations associated with simple baroclinic waves in a two-level quasi-geostrophic model. *Tellus*, **6,** 273–286.

Physick, W. L., 1981: Winter depression tracks and climatological jet streams in the Southern Hemisphere during the FGGE year. *Quart. J. Roy. Meteor. Soc.*, **107,** 883–898.

Simmonds, I., and Y. Lin, 1983: Topographic and thermal forcing in a general circulation model of the Southern Hemisphere—January case. The University of Melbourne Meteor. Dept. Pub. No. 24, 88 pp.

Taljaard, J. J., H. van Loon, H. L. Crutcher and R. L. Jenne, 1969: *Climate of the Upper Air: Southern Hemisphere,* Vol. 1. NAVAIR 50-IC-55.

Trenberth, K. E., 1979: Interannual variability of the 500 mb zonal mean flow in the Southern Hemisphere. *Mon. Wea. Rev.*, **107,** 1515–1524.

——, 1980: Planetary waves at 500 mb in the Southern Hemisphere. *Mon. Wea. Rev.*, **108,** 1378–1389.

——, 1981: Observed Southern Hemisphere eddy statistics at 500 mb: Frequency and spatial dependence. *J. Atmos. Sci.*, **38,** 2585–2605.

——, 1982: Seasonality in Southern Hemisphere eddy statistics at 500 mb. *J. Atmos. Sci.*, **39,** 2507–2520.

——, 1984: Interannual variability of the Southern Hemisphere circulation: Representativeness of the year of the Global Weather Experiment. *Mon. Wea. Rev.*, **112,** 108–123.

van Loon, H. R., 1972: Wind in the Southern Hemisphere. *Meteorology of the Southern Hemisphere. Meteor. Monogr.*, No. 35, C. W. Newton, Ed., Amer. Meteor. Soc., 87–99.

——, 1980: Transfer of sensible heat by transient eddies in the atmosphere on the Southern Hemisphere: An appraisal of the data before and during FGGE. *Mon. Wea. Rev.*, **108,** 1774–1781.

Webster, P. J., and D. G. Curtin, 1974: Interpretations of the EOLE experiment. Part I: Temporal variation of Eulerian quantities. *J. Atmos. Sci.*, **31,** 1860–1875.

——, and ——, 1975: Interpretations of the EOLE experiment. Part II: Spatial variation of Eulerian quantities. *J. Atmos. Sci.*, **32,** 1848–1863.

White, G. H., 1982: An observational study of the Northern Hemisphere extratropical summertime general circulation. *J. Atmos. Sci.*, **39,** 24–40.